ARTICLES SCIENCE CHINA Materials

mater.scichina.com link.springer.com

Published online 31 July 2019 | https://doi.org/10.1007/s40843-019-9473-2
Sci China Mater 2019, 62(12): 1888–1897

Advanced 3D nanohybrid foam based on graphene oxide: Facile fabrication strategy, interfacial synergetic mechanism, and excellent photocatalytic performance

Xiaoyuan Zhang[1†], Wenfeng Wei[1†], Shan Zhang[1], Bianying Wen[2*] and Zhiqiang Su[1*]

ABSTRACT **Herein, a unique nanohybrid foam was fabricated with titanium dioxide (TiO_2)-carbon quantum dots (CQDs) nanoparticles intercalated between graphene oxide (GO) layers *via* a facile and low-cost solvothermal method. Compared with pure GO foam, the fabricated GO-TiO_2-CQDs foam displayed high degradation rate towards methyl orange (MO), methylene blue (MB), and rhodamine B (RhB), respectively, under the Xenon lamp irradiation. The composite foam can be used for several times and remain a high degradation rate without structural damage. The photochemical property was attributed to the 3D porous structure of GO-TiO_2-CQDs foam, in which ultrafine hydrogenated TiO_2-CQDs nanoparticles were densely anchored on the GO sheets. This paper provides an efficient strategy to tune the charge transport and thus enhance the photocatalytic performance by combining the semi-conductive GO and quantum dots.**

Keywords: graphene, titanium dioxide, carbon quantum dots, nanohybrid foam, photocatalytic degradation

INTRODUCTION

With the increasing environmental contamination over recent years, photocatalyst materials have attracted much attention due to their controllable and adjustable properties. Photocatalysis is a simple process to degrade water pollution with high reactivity by photocatalysts under mild reaction conditions. Photocatalysts can convert light into chemical energy, thus promoting the oxidization or reduction of the pollutants [1,2]. The primary requirement for the photocatalysts is that there is sufficient energy to induce a catalytic chemical reaction. Among all the photocatalysts, metal oxide semiconductors such as zinc oxide (ZnO, E_g=3.2 eV) [3,4], ferric oxide (Fe_2O_3, E_g =3.2 eV) [5], titanium dioxide (TiO_2, E_g=3.2 eV) [6], cuprous oxide (Cu_2O, E_g=2.2 eV) [7–9], and tin oxide (Sn_2O_3, E_g=3 eV) [10,11] are recognized as the efficient degraders for organic dyes. The photo-generated electrons and holes from the photocatalysts can interact with the surrounding environment to produce superoxide radicals or hydroxyl radicals. These radicals have strong oxidative properties and can degrade pollutants in water. These metal oxides have been widely investigated for photocatalysis [7], Li-ion battery [12], and supercapacitors [13], due to their large specific surface area and excellent electrochemical activity.

The cost-effective TiO_2 is an outstanding candidate for the photocatalyst owing to its superior properties, including chemical stability, durable oxidizing power, and nontoxicity [14]. Zhang *et al.* [15] fabricated a water-dispersible TiO_2/graphene nanocomposite *via* a facile and efficient hydrothermal approach. TiO_2 can generate highly active electrons and holes to react with oxygen in water, and further degrade organic dyes in water. It was noticed that the architectures of the TiO_2, including nanosphere [16], nanotube [17], nanowire [18], and nanosheet [19], influence the physicochemical properties of

[1] State Key Laboratory of Chemical Resource Engineering, Beijing Key Laboratory of Advanced Functional Polymer Composites, Beijing University of Chemical Technology, Beijing 100029, China
[2] Beijing Key Laboratory of Quality Evaluation Technology for Hygiene and Safety of Plastics, Beijing Technology and Business University, Beijing 100048, China
† These authors contributed equally to this work.
* Corresponding authors (emails: suzq@mail.buct.edu.cn (Su Z); wenbianying@tsinghua.org.cn (Wen B))

the photocatalysts. Reports showed that combining TiO_2 with other semiconductor nanomaterials could effectively improve the photocatalysis *via* the interfacial charge-transfer processes of the photo-generated charge carriers [6]. Notably, conductive carbonaceous materials, such as graphene and carbon quantum dot (CQD), were integrated with TiO_2 to adjust the band gap and enhance the charge transfer rate of the nanocomposites [20,21]. Sathish Kumar *et al.* [22] obtained CQD/TiO_2 nanohybrids *via* a simple one-step solvothermal method. The CQD/TiO_2 exhibited high decomposition rate of methylene blue (MB), due to the fast charge transfer between CQD and TiO_2. CQDs can promote the interfacial charge, energy transfer, and relaxation processes, and thus enhance the photocatalytic performance of TiO_2. Other than CQDs, graphene exhibits sizeable specific surface area and excellent electrical conductivity. Yang *et al.* [23] fabricated TiO_2 with different dimensions by *in-situ* synthetic strategies and then hybrided them with graphene. Graphene plays a substantial role in collecting photoexcited electrons from the conduction band of TiO_2 and prevents the recombination of electrons and holes generated inside or on the surface of the TiO_2 [7]. Different constructions of nanocomposites expand the scope of photocatalysis [24–26]. Lee *et al.* [27] demonstrated that graphene wrapped amorphous TiO_2 nanoparticles possessed excellent photocatalytic properties under visible light for the degradation of MB.

In this study, the three-dimensional (3D) hybrid foam composed of TiO_2-CQDs nanoparticles and graphene oxide (GO) nanosheets was fabricated *via* the hydrothermal method as shown in Scheme 1. Compared with powders and membranes of graphene and TiO_2 nanocomposites, 3D graphene foam displays high elasticity and mechanical stability, excellent electrochemical stability, and high conductivity, due to the well interconnected porous microstructure in the nanocomposites, which benefit the adsorption of contaminant and the hybrid of electrodes [12,28–30]. Deng *et al.* [31] obtained GO sheets with different lateral sizes by controlling the delamination conditions of graphite oxide with a convenient one-step hydrothermal self-assembly method. In our system, graphene was utilized to integrate with TiO_2-CQDs nanoparticles and then form a 3D structure to promote efficient charge separation. This study provides a new opportunity for developing reusable and high-performance photocatalyst for wastewater treatment.

EXPERIMENTAL SECTION

Materials

Natural graphite flake (99.8% purity) and glucose (99.5% purity) were purchased from Sigma Aldrich. Potassium permanganate ($KMnO_4$) and absolute ethanol were purchased from Beijing Chemicals Co., Ltd (Beijing, China). Sulfuric acid (H_2SO_4, analytical grade, 98% aqueous solution), phosphoric acid (H_3PO_4, analytical grade, 35% aqueous solution), and hydrogen peroxide (H_2O_2, analytical grade, 30% aqueous solution) were bought from Tianjin Dongfang Chemical Plant (Tianjin, China). TiO_2 (analytical grade, P25), thiourea, rhodamine B (RhB), methyl orange (MO), and MB were purchased from J&K (Beijing, China). All the chemicals were used without additional purification. The deionized water was obtained by a Millipore system (≈18.2 MΩ cm^{-1}).

Preparation of TiO_2-CQDs nanocomposites

Firstly, CQDs were fabricated *via* a one-pot hydrothermal method [32]. In detail, 2 g glucose was dissolved in 20 mL deionized water. Then, the solution was transferred into a Teflon-lined stainless steel autoclave for hydrothermal reaction at 200°C for about 10 h to obtain the CQDs.

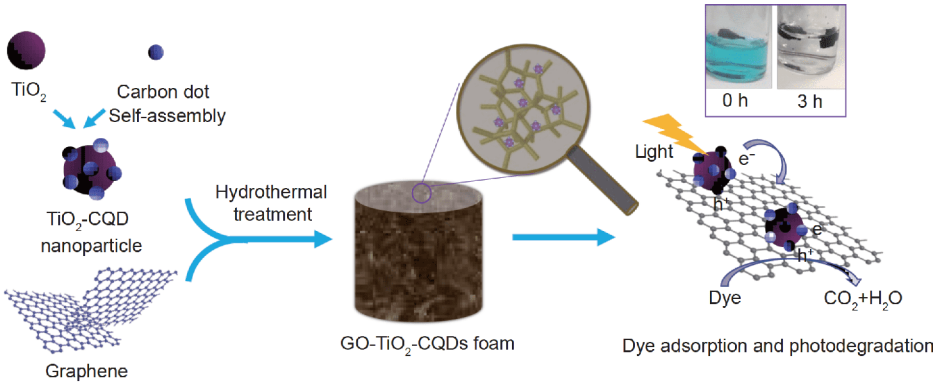

Scheme 1 Schematic of the preparation of GO-TiO_2-CQDs foam.

Then, the CQDs were anchored on the surfaces of TiO_2 nanoparticles with a primary particle size of 25 nm by stirring TiO_2 (100 mg) with a pre-determined amount of CQDs in 30 mL deionized water for 30 min. The solution became a homogeneous light brown suspension without visible precipitation, and then was transferred into a Teflon-lined stainless steel autoclave for hydrothermal reaction about 10 h at 200°C. Then, the solution was cooled at ambient temperature, and a dark brown liquid was obtained. The composites were isolated by centrifugation and dried under vacuum at 60°C.

Preparation of GO

GO was synthesized according to the modified Hummers method [33]. Specifically, 40 mL concentrated phosphoric acid and 360 mL sulfuric acid were slowly injected into 3 g of natural graphite flakes under stirring at ambient temperature. Then 18 g potassium permanganate was added slowly into the system in the water bath for 12 h (50°C). After cooled down to 25°C, the mixture was slowly poured onto 200 mL ice crush and 5 mL 10% hydrogen peroxide. Then the luminous yellow solution was centrifuged for 30 min (4000 rpm). The precipitation was then washed with water, 30% hydrochloric, and ethanol (2×), respectively. Subsequently, the obtained suspension was filtered through a polytetrafluoroethylene (PTFE) membrane (pore size: 0.22 μm) using diethyl ether as the solvent. After vacuum-drying for 12 h, the GO was obtained.

Preparation of GO-TiO_2-CQD foam

The GO-TiO_2-CQDs foam was fabricated by hydrothermal treatment. Firstly, 20 mg TiO_2-CQD nanoparticles were dispersed in 30 mL homogeneous GO (2 mg mL^{-1}) suspension. After the addition of 1 g thiourea, the mixture was sonicated for 30 min. Next, the mixture was transferred into a 50-mL Teflon-lined stainless steel autoclave and maintained at 180°C for 4.5 h. After natural cooling, the GO-TiO_2-CQD foam was soaked in distilled water for 24 h along with three times of water change to remove residual gas and other impurities. Finally, vacuum freeze-drying was used to remove water and the GO-TiO_2-CQD foam was obtained. The preparation of pure graphene foam was to disperse GO into 30 mL suspension with the assistance of 1 g thiourea. After ultrasonic dispersion, the mixture was transferred into a 50-mL Teflon-lined stainless steel autoclave under the same hydrothermal conditions and operation steps. To obtain GO-TiO_2 foam, 1 g thiourea and 100 mg TiO_2 powder were dispersed into 30 mL suspension of GO. After ultrasonic dispersion, the mixture was transferred into a 50-mL Teflon-lined stainless steel autoclave under the same hydrothermal conditions and operation steps.

Photodegradation of organic dyes

The photodegradation behaviors of the hybrids were measured with MB, RhB, and MO. They were mixed just before the degradation experiments. The foam (15 mg) was immersed into 4.5 mL MB, RhB, and MO solution (10 μmol L^{-1}), respectively. Photocatalysis was carried out under the irradiation of the Xenon lamp of 150 W. The absorbance of the reaction solution was monitored in real time, and each data was repeated for three times to get the average value. The foams after the dye absorption were soaked in 5 mL ethanol solution for desorption, and the absorbance of the solution was measured every half an hour. During the desorption process, the ethanol solution gradually changed from colorless to the color of the dye, until the color of the solution no longer varied, indicating that the dye was entirely desorbed and the foam can be reused.

Characterization

The scanning electron microscopy (SEM) images of the TiO_2-CQDs nanoparticles and GO-TiO_2-CQDs foam were obtained by using the JSM-6700F (JEOL, Japan). The transmission electron microscopy (TEM) images were acquired on a JEM-2100F(JEOL, Japan) at the acceleration voltage of 200 kV. The TiO_2-CQDs nanohybrids aqueous solution was dropped onto the copper grid and dried at room temperature. X-ray diffraction (XRD) was taken on a Rigaku D/max-2500 VB+/PC(JEOL, Japan) equipment with the scanning 2θ angle from 5° to 90°. X-ray photoelectron spectroscopy (XPS) was performed on thermo VG (ESCALAB 250, Waltham, USA). Raman spectroscopy was recorded by a Raman spectroscope (LabRAM HORIBA JY, Edison, NJ). The solid powder and foam were placed directly on a quartz glass slide, and the laser focus position was adjusted before testing. Fourier transform infrared spectroscopy (FTIR) was recorded using a Nicolet NEXUS (Nicolet 6700, Thermo-Fisher, USA) instrument with transmission accessory. The atmospheric background was collected before each scan. The samples were prepared by potassium bromide (KBr) tableting method. The samples of TiO_2-CQD and GO-TiO_2-CQD were ground uniformly with KBr according to the ratio of 1:100 in an agate mortar. And then they were tested by transmission plug. The concentration of dyes during the photodegradation was characterized by UV-vis (PerkinElmer, Lambda 365,

Korea) absorbance measurement.

RESULTS AND DISCUSSION

Morphology of GO-TiO_2-CQD foam

The morphological changes of TiO_2-CQDs nanoparticles were characterized by SEM, shown as the images of the TiO_2 nanoparticles before and after CQD decoration, with TiO_2@glucose as the reference to identify the function of CQD in the nanocomposite, and decrease the uncertainty from the addition of glucose. It can be found that the irregular nanoparticles formed when the TiO_2 nanoparticles were directly mixed with glucose (Fig. 1a). However, after decorating the CQDs, the obtained TiO_2-CQDs display satellite structure with the surface nanoparticle size ranging from 50 to 100 nm (Fig. 1b, c).

Moreover, the CQDs on the surface of TiO_2-CQDs reduced the aggregation and resulted in a better dispersion of TiO_2. The –OH functional groups on the surface of the TiO_2 can anchor on the surface of CQDs, leading to the satellite structure of TiO_2-CQDs with the alternating arrangement of TiO_2 and CQDs. As shown in Fig. 1d–e, the TiO_2-CQDs contain only three elements, C, O, and Ti, indicating that most of the surface elements are CQDs, and the content of Ti element is only 0.1%.

The morphology of the prepared GO and GO-TiO_2-CQDs foam was characterized and shown in Fig. 2a, b. It can be seen that GO foam is stacked by many lamellas with many uneven holes. The size of the hole can be adjusted based on the concentration of graphene. The internal hole is more uniform and has a relatively stable structure when the concentration of graphene is 2 mg mL^{-1}. The lower concentration of the original solution, the higher the specific surface area of the foam. However, the structure is loose, and the mechanical property is poor in hybrid foam with low graphene concentration. Therefore, the concentration of graphene in 2 mg mL^{-1} was selected for the subsequent experiments. In the hydrothermal preparation process of the foam, thiourea was decomposed into ammonia and hydrogen sulfide, which could further exfoliate GO into single layer and reduce GO. Besides, these compounds decorated on the surface of GO, so that the stacking between the adjacent layers became more compact *via* π-π stacking, electrostatic interaction and hydrogen bonds. However, a larger content of thiourea will not lead to stable GO foam because of the gas molecules release. Therefore, 1.0 g thiourea was applied in the experiment. In Fig. 2c, d, the SEM images of GO-TiO_2-CQDs foam show that the addition of TiO_2 does not affect the microporous structure of GO, but help to form aggregates at nanoscale, which significantly increases the specific area of foam. Also, we found the nanoparticles did not fall off even when they were immersed in deionized water for several days. This indicates that the TiO_2-CQDs nanoparticles are successfully loaded on the graphene layers through electrostatic interaction and hydrogen bonds.

Structural analysis of GO-TiO_2-CQD foam

The change of functional groups before and after the combination of TiO_2 with CQDs was explored by UV-vis testing in Fig. 3a. The absorption band at 226 nm is as-

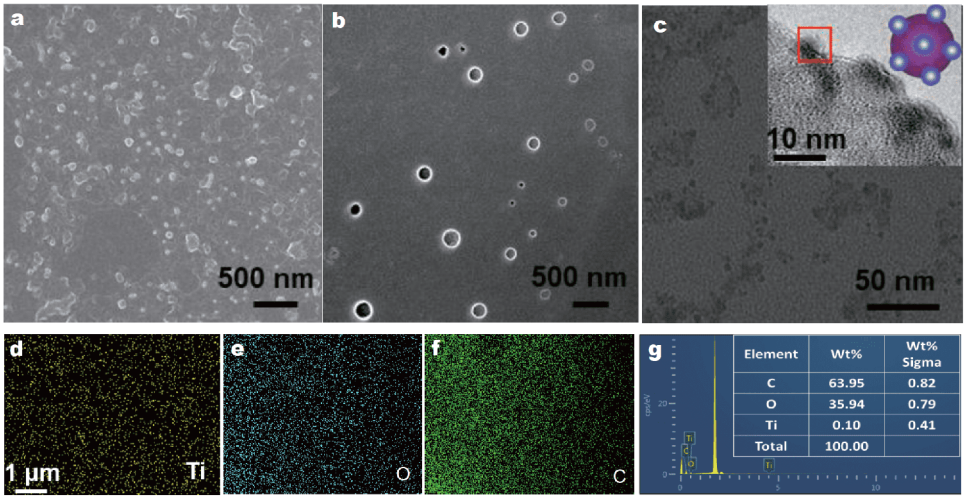

Figure 1 SEM images of TiO_2@glucose (a) and TiO_2-CQDs (b); (c) TEM and HRTEM images of TiO_2-CQDs; (d–f) elemental analyses of TiO_2-CQDs; (g) elemental analysis of TiO_2-CQDs prepared by hydrothermal method.

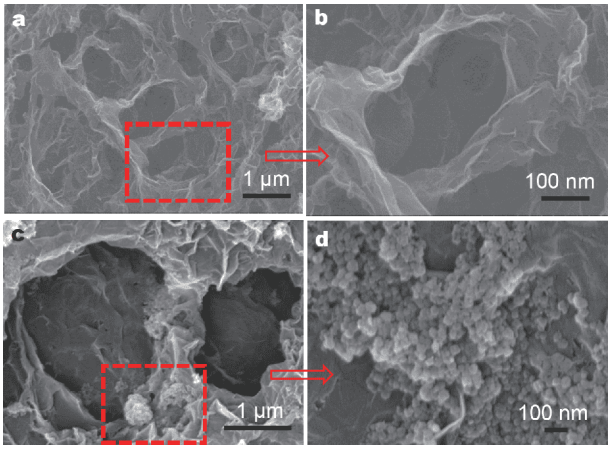

Figure 2 (a) SEM image of GO foam and (b) GO foam with larger magnification; (c) SEM image of GO-TiO_2-CQDs foam and (d) foam with larger magnification.

cribed to n→σ*, which can be observed in all three UV-vis curves of CQDs, TiO_2 and TiO_2-CQDs, verifying the existence of –OH. When the composite nanoparticles form, the absorption peak slightly decreases relative to CQDs and TiO_2, indicating the change of –OH content. Another peak, the R band, near 280 nm is ascribed to n→π*, which can be seen in the UV-vis curves of CQDs and TiO_2-CQDs. Due to the dehydration at high temperature, some oxygen functional groups of glucose and –OH on the surface of TiO_2 powder turn into C=O. Besides, the inserted optical images of TiO_2-CQDs under the natural light and the 365 nm ultraviolet light are also shown in Fig. 3a. As the specific color enhancement effect presents, the CQDs system is stabilized by the hybrid with TiO_2. It can be observed that there is a slight blue fluorescence under 365 nm ultraviolet light.

Fig. 3b shows the photoluminescence spectra of TiO_2, CQDs and TiO_2-CQDs nanoparticles. Due to the aggregation of hydroxyl groups on the surface of TiO_2 in water, the most active emission wavelength of pure TiO_2 is about 390 nm when the excitation wavelength is 260 nm, while the most vigorous emissions of anatase and rutile locate at 378 and 400 nm, respectively. For CQD and TiO_2-CQDs, by scanning the emission spectra at different excitation wavelengths, we can see that the most active excitation wavelength is about 340 nm, and the corresponding emission wavelength is about 430 nm. The anchoring of TiO_2 results in the increase of fluorescence peak intensity at 430 nm, indicating that the broadband gap of TiO_2 affects the surface structure of CQDs, not the photoluminescence property. It can be assumed that, when the excitation light irradiates, a part of the electrons transfer to the CQDs, leading to the charge separation of the photogenerated electrons and holes in the TiO_2. Generally, the band gap of TiO_2 is about 3.0–3.2 eV, while the electron and hole easily recombine, limiting its application in catalysis. The CQDs, as a kind of photosensitive material, can effectively guide the electron transfer of TiO_2, resulting in effective inhibition of electron and hole recombination. Therefore, electron and holes on the CQDs react with O_2 and H_2O to form superoxide anion ($O_2^{\bullet-}$) and hydroxyl radical ($HO^{\bullet}$).

In Fig. 3c, the zeta potential of pure CQDs is unstable and displays a broad fluctuation range. Finally, it tends to stabilize at −20 mV, where the CQDs are prone to aggregate. The pure TiO_2 shows relatively stable zeta potential of 25 mV. While for TiO_2-CQDs, the variation of zeta potential is within 40–80 mV in steady state. The positive charge on the surface of TiO_2-CQDs makes them easily assemble with GO. Fig. 3d shows the Raman spectra of the TiO_2, CQDs, and TiO_2-CQDs to elucidate the structural complexity of TiO_2-CQDs, according to the separated peaks from different phases. The modes, A_{1g} (492 cm^{-1}), B_{1g} (412 and 492 cm^{-1}), and E_g (144, 209, and 630 cm^{-1}), are six fundamental transitions of anatase. The four modes, A_{1g} (614 cm^{-1}), B_{1g} (143 cm^{-1}), B_{2g} (822 cm^{-1}), and E_g (432 cm^{-1}), are Raman-active modes of rutile. Therefore, the Raman spectra show the co-excitation of rutile and anatase TiO_2 phases. The intensity of the observed peaks also indicates that the anatase is predominant.

The structural transitions of GO foam and GO-TiO_2-CQDs foam are confirmed by FTIR, Raman, and XRD. As

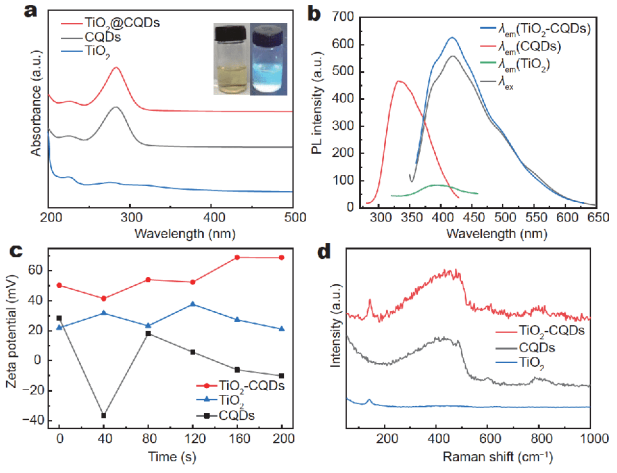

Figure 3 UV-vis spectra (a), fluorescence spectra (b), zeta potential (c) of TiO_2, CQDs and TiO_2-CQDs, and Raman shift (d) of TiO_2, CQDs and TiO_2-CQDs.

shown in Fig. 4a, FTIR spectra indicate that both the GO foam and GO-TiO_2-CQDs foam have some oxygen-containing groups, such as –OH (3446 and 1442 cm^{-1}), C=O (1639 cm^{-1}), and C–O–C (1110 cm^{-1}). Moreover, the peaks at 2850 and 2925 cm^{-1} correspond to $-CH_2$ symmetry and antisymmetric stretching vibration. The vibrational peaks of the oxygen-containing functional groups are weakened, indicating that the high-temperature process results in the dehydration and reduction of the GO. Moreover, a typical skeletal vibration of Ti–O–Ti bonds near 522 cm^{-1} in GO-TiO_2-CQD foam can be observed, further confirming that TiO_2 is chemically bonded to CQDs and GO, not only physical adsorption.

In the Raman spectra (Fig. 4b), the peaks of the D band at 1305 cm^{-1} and the G band at 1579 cm^{-1} are more obvious in GO-TiO_2-CQDs foam, indicating that the GO is stripped at high temperature and new defects introduced. The I_D/I_G of GO foam increases from 1.10 to 1.23 for GO-TiO_2-CQDs foam, confirming the introduction of new defects in GO-TiO_2-CQDs foam. The other peaks at 599 and 590 cm^{-1} are ascribed to symmetric and antisymmetric expansion vibration of Ti–O. The peak at 807 cm^{-1} is ascribed to the lattice defects indicating the presence of NH_3. The peak at 1061 cm^{-1} is ascribed to the antisymmetric stretching vibration of $-SO_3H$. Fig. 4c presents XRD patterns of the GO foam and GO-TiO_2-CQDs foam. In the XRD pattern of GO-TiO_2-CQDs foam, the peaks at 2θ of 25.5°, 37.2°, 37.88°, 48.14°, 53.94°, 55.14°, 62.88°, 68.86°, 70.36°, 75.18°, and 82.86° can be assigned to the (101), (103), (004), (200), (105), (211), (204), (116), (220), (215), and (224) of the anatase TiO_2, respectively, in good agreement with the standard JCPDS card No. 028-1192.

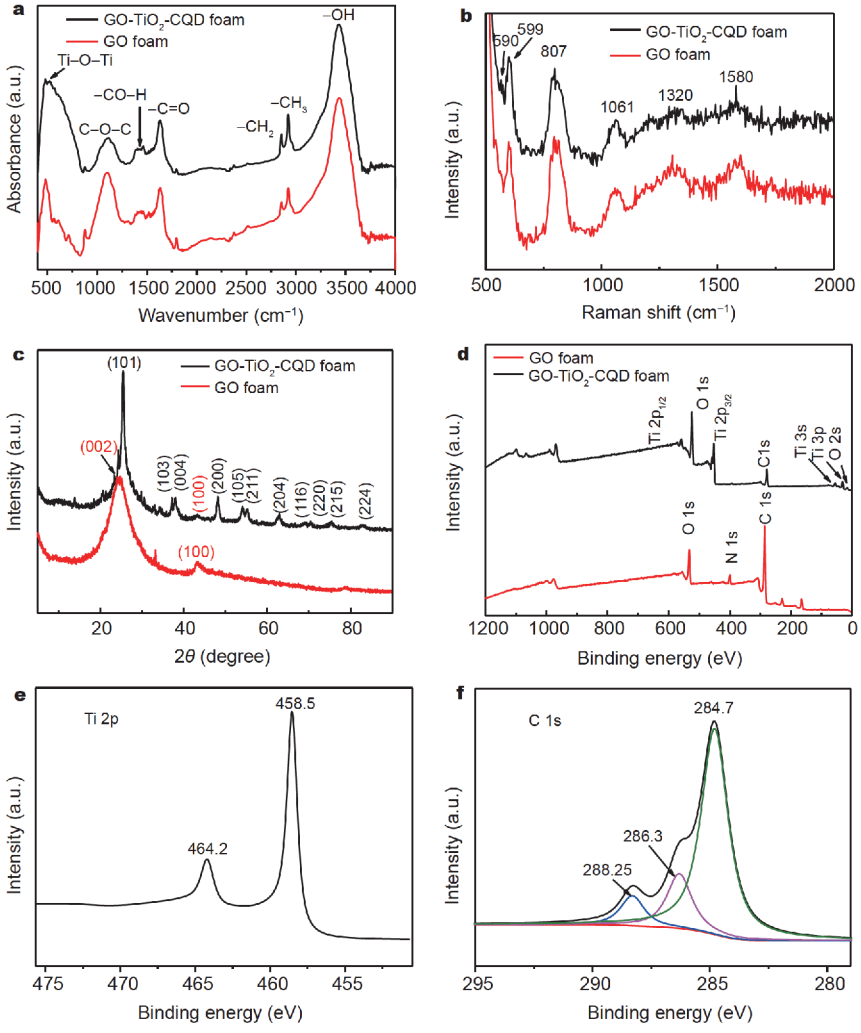

Figure 4 FTIR (a), Raman shift (b), XRD patterns (c) and XPS spectra (d) of GO foam and GO-TiO_2-CQD foam. The Ti 2p peaks (e) and the C1s peaks (f) of GO-TiO_2-CQD foam.

This proves that TiO_2 in the GO-TiO_2-CQDs foam is mainly in the form of anatase. The typical (002) peak located at 24.6° demonstrates the disorder stacking structure of GO layers. The weak broad (001) peak at 9.7° implies the existence of a small amount of oxygen-containing groups.

From Fig. 4d, the XPS spectra of GO foam show bands located at 534, 400 and 285 eV, which are associated with the characteristic peak of O 1s, N 1s, and C 1s, respectively. The peak at about 400 eV can be attributed to the formation of amino and amide groups due to the decomposition of thiourea. Meanwhile, the XPS spectrum of the synthesized GO-TiO_2-CQD foam shows three predominant binding energy peaks around 524, 453 and 278 eV, corresponding to the C 1s, Ti 2p, and O 1s, respectively. As shown in Fig. 4e, the Ti 2p spectrum shows two peaks at the binding energy of 464 and 459 eV, corresponding to Ti $2p_{3/2}$ and Ti $2p_{1/2}$, respectively [28]. The C 1s spectrum in Fig. 4f consists of two binding energy peaks at 288 and 286 eV, assigned to the oxygen bound species C–O and C=O, respectively. Another absolute peak at 284.7 eV corresponds to the none-oxygenated ring C atom (C=C/C–C).

Photocatalytic properties of the synthesized 3D foam for organic dyes

The photocatalytic activities of the foam were investigated by adsorbing MO, RhB, and MB. The photocatalytic degradations of MO over the GO foam, GO-TiO_2 foam, and GO-TiO_2-CQDs foam were detected by UV-vis spectroscopy. MO displays orange color in water and absorbs in the visible region at 466 nm. Based on the Lambert-Bill law, a linear relationship between the absorbance and the concentration of the dye solution is assumed. Here, the photocatalytic degradation rate (D%) is defined as the following formula [34]:

$$D\% = \frac{(A_0 - A_T) \times 100\%}{A_0}.$$

Therein, A_0 is the absorbance of the original solution, and A_T is the absorbance at T min. Fig. 5a–c show the time-dependent UV-vis spectra of MO in the presence of the GO foam, GO-TiO_2 foam and GO-TiO_2-CQDs foam in a neutral aqueous solution under Xenon lamp irradiation. The absorbance intensity of MO gradually decreases as a function of time under irradiation. As shown in Fig. 5d, the corresponding degradation efficiencies for GO foam, GO-TiO_2 foam, GO-TiO_2-CQDs foam, and TiO_2 powder are about 68.37%, 81.57%, 92.47%, and 13.85%, respectively. The faster and higher degradation of MO was observed in the presence of the GO-TiO_2-CQDs foam. After 3 h, the color of aqueous MO solution with GO-TiO_2-CQDs foam almost disappears (Fig. 5c inset). This phenomenon indicates that not only the GO foam, but also the TiO_2-CQDs nanoparticles have specific catalytic degradation effect on dyes.

Also, the degradation experiments were carried out on RhB and MB with GO foam, GO-TiO_2 foam, and GO-TiO_2-CQDs foam. The time-dependent degradation curves are shown in Fig. 5e. The GO-TiO_2-CQDs foam displays a stronger degradation rate (95.54%) to MB than GO-TiO_2 foam (85.46%), GO foam (81.95%) and TiO_2 powder (30.99%). Similar to MO and MB, when GO foam, GO-TiO_2 foam, and TiO_2 powder were added to RhB solution, the degradation efficiencies were 68.41%, 75.96%, and 25.50%. However, when GO-TiO_2-CQDs foam was added, the degradation efficiency was increased to 92.84% (Fig. 5f). The slope of the photocatalysis degradation kinetic curve illustrates that the GO-TiO_2-CQDs foam has a faster degradation rate and higher degradation efficiency towards MB (Fig. 5d–f), which may be attributed to the stronger electrostatic adsorption effects aroused by the more considerable negative surface potential of MB. The recycling degradation experiments using GO foam, GO-TiO_2 foam, and GO-TiO_2-CQDs foam were performed under the same conditions. As shown in Fig. 5g–i, the degradation efficiencies of MB, MO, and RhB all maintain at a high level for GO foam, GO-TiO_2 foam, and GO-TiO_2-CQDs foam.

Combined with the explanation of photocatalytic effect in the previous work [22,35], the photocatalytic elucidation of the GO-TiO_2-CQDs foam is schematically shown in Scheme 2. Pairs of electrons and holes are produced when photocatalyst TiO_2 nanoparticles absorb UV radiation from Xenon lamp. As the results of FL-testing show, the combination of TiO_2 and CQDs can effectively transfer the photogenerated electrons generated by TiO_2 to the surface of carbon dots. In detail, parts of negative-electrons (e^-) are easily transferred to CQDs, and the other parts of negative-electrons (e^-) transfer to GO. Thereby, the lifetime of photogenerated electrons is increased, and the photocatalytic effect is improved.

Moreover, these electrons react with oxygen in the water to form superoxide anion ($O_2^{\bullet -}$) for further oxidizing dyes. On the other hand, the positive-holes (h^+) left behind by the electron transfer on TiO_2 will react with water to form hydroxyl radicals ($OH^\bullet$). The hydroxyl radicals can oxidize dyes and finally mineralize them into the water and harmless inorganics. Interestingly, by transferring electrons out of TiO_2 to GO or CQDs, the combination of negative-electrons (e^-) and the positive-

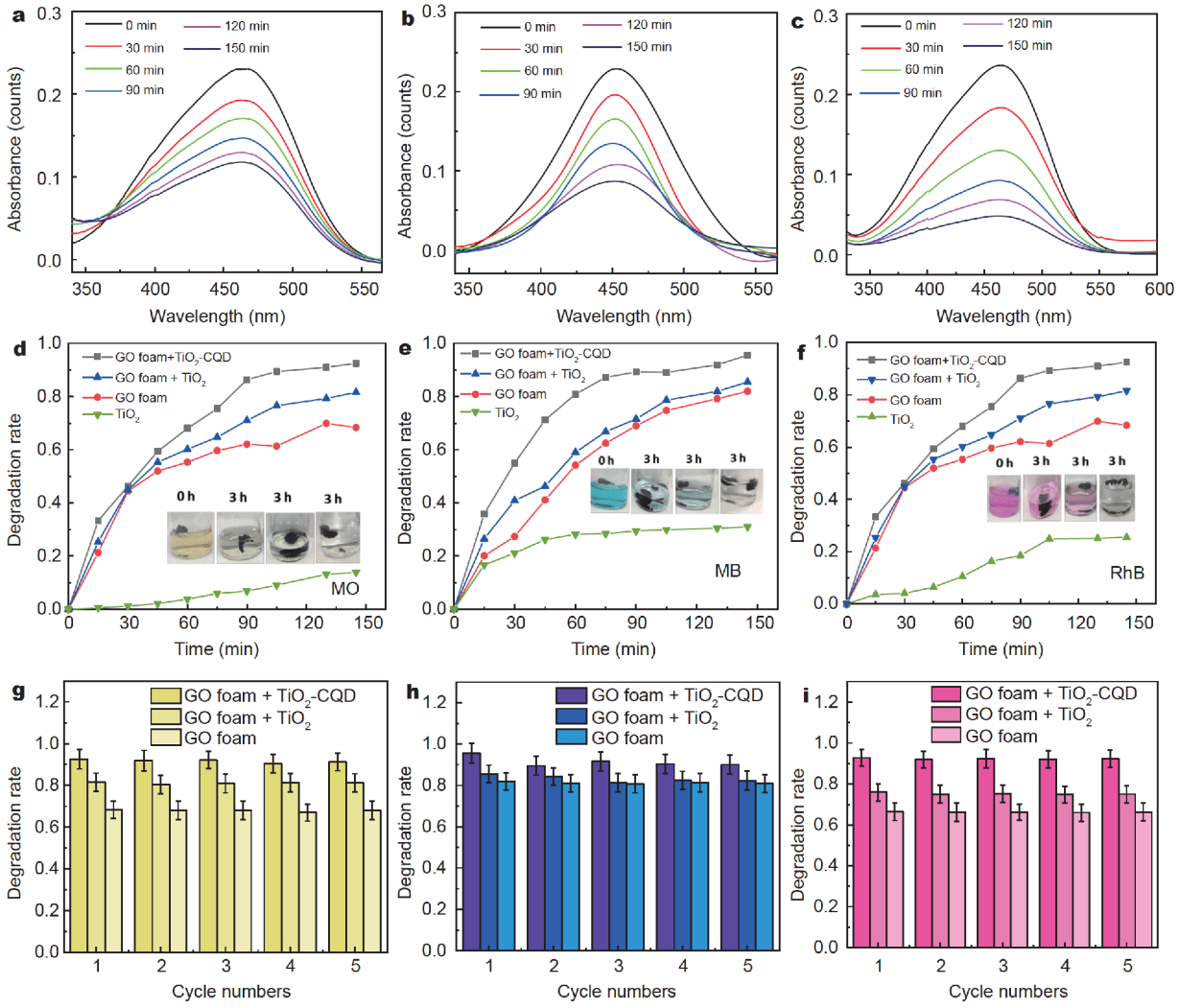

Figure 5 UV-vis spectra of MO degradation with GO foam (a), GO-TiO_2 foam (b) and GO-TiO_2-CQDs foam (c) with different irradiation times; photocatalytic degradation kinetics of MO (d), MB (e), RhB (f) and the relevant optical image of the degradation with GO foam, GO-TiO_2 foam, GO-TiO_2-CQD foam and TiO_2 powder after 3 h; the error for each data point is not more than 5%, photocatalysis degradation rates of MO (g), MB (h) and RhB (i) at different cycles.

hole (h^+) could effectively improve the photocatalytic efficiency of GO-TiO_2-CQDs foam. Compared with the previous reported TiO_2 nanoparticles only combined with GO or CQD, this 3D foam can more effectively improve the transfer rate of photogenerated electrons and promote the separation of electrons and holes to improve the photocatalytic effect.

CONCLUSIONS

In summary, a novel photoactive GO-TiO_2-CQDs composite, consisting of GO, CQD, and TiO_2, was fabricated *via* a facile and efficient solvothermal route. This GO-TiO_2-CQDs composite displays a 3D foam structure, in which TiO_2-CQDs microspheres adsorb on porous graphene sheets. Compared with pure GO foam, the fabricated GO-TiO_2-CQDs foam displays high degradation rates of 92.48%, 95.54%, and 92.84% towards MO, MB, and RhB, respectively, under the Xenon lamp irradiation. This indicates that the high degradation efficiency benefits from the GO sheets, which can accept electrons and inhibit charge recombination between the electrons in the conduction band of TiO_2 and holes in the valence band of CQDs. Besides, GO-TiO_2-CQDs foam maintains the high photodegradation rate after being used for several times, indicating the remarkable degradation capability and stability. The encouraging performances indicate that the

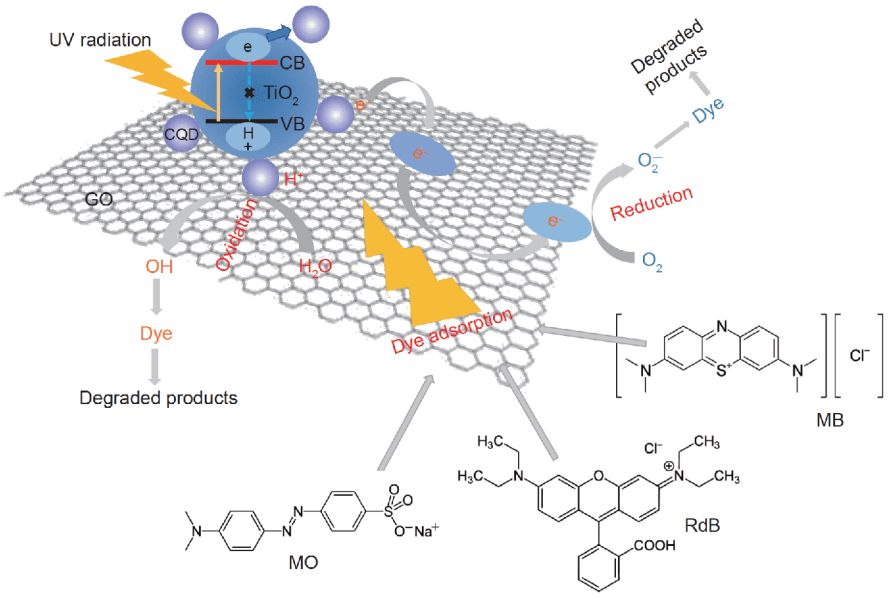

Scheme 2 Photocatalytic degradation mechanism of the synthesized GO-TiO_2-CQDs foam on organic dyes under Xenon lamp irradiation.

obtained GO-TiO_2-CQDs foam may have a promising prospect as photocatalyst. More broadly, our 3D foam provides photogenerated electrons with strong reduction ability and photoelectron with strong reduction ability under Xenon lamp. Therefore, this 3D platform is expected to be used for the preparation of hydrogen by high efficient photolysis of water.

Received 1 June 2019; accepted 7 July 2019; published online 31 July 2019

1 Liu W, Liu Z, Wang G, *et al.* Carbon coated Au/TiO_2 mesoporous microspheres: A novel selective photocatalyst. Sci China Mater, 2017, 60: 438–448
2 Yang X, Tian L, Zhao X, *et al.* Interfacial optimization of g-C_3N_4-based Z-scheme heterojunction toward synergistic enhancement of solar-driven photocatalytic oxygen evolution. Appl Catal B-Environ, 2019, 244: 240–249
3 Pacholski C, Kornowski A, Weller H. Site-specific photodeposition of silver on ZnO nanorods. Angew Chem Int Ed, 2004, 43: 4774–4777
4 Ding J, Zhu S, Zhu T, *et al.* Hydrothermal synthesis of zinc oxide-reduced graphene oxide nanocomposites for an electrochemical hydrazine sensor. RSC Adv, 2015, 5: 22935–22942
5 Sun K, Wang L, Wu C, *et al.* Fabrication of α-Fe_2O_3@rGO/PAN nanofiber composite membrane for photocatalytic degradation of organic dyes. Adv Mater Interfaces, 2017, 4: 1700845
6 Tian J, Zhao Z, Kumar A, *et al.* Recent progress in design, synthesis, and applications of one-dimensional TiO_2 nanostructured surface heterostructures: A review. Chem Soc Rev, 2014, 43: 6920–6937
7 Almeida BM, Melo Jr. MA, Bettini J, *et al.* A novel nanocomposite based on TiO_2/Cu_2O/reduced graphene oxide with enhanced solar-light-driven photocatalytic activity. Appl Surf Sci, 2015, 324: 419–431
8 Ding J, Sun W, Wei G, *et al.* Cuprous oxide microspheres on graphene nanosheets: An enhanced material for non-enzymatic electrochemical detection of H_2O_2 and glucose. RSC Adv, 2015, 5: 35338–35345
9 Zhao X, Li Y, Guo Y, *et al.* Coral-like MoS_2/Cu_2O porous nanohybrid with dual-electrocatalyst performances. Adv Mater Interfaces, 2016, 3: 1600658
10 Gao C, Li X, Lu B, *et al.* A facile method to prepare SnO_2 nanotubes for use in efficient SnO_2–TiO_2 core–shell dye-sensitized solar cells. Nanoscale, 2012, 4: 3475–3481
11 Cui S, Wen Z, Huang X, *et al.* Stabilizing MoS_2 nanosheets through SnO_2 nanocrystal decoration for high-performance gas sensing in air. Small, 2015, 11: 2305–2313
12 Yu X, Lin D, Li P, *et al.* Recent advances in the synthesis and energy applications of TiO_2-graphene nanohybrids. Sol Energy Mater Sol Cells, 2017, 172: 252–269
13 Dong X, Cao Y, Wang J, *et al.* Hybrid structure of zinc oxide nanorods and three dimensional graphene foam for supercapacitor and electrochemical sensor applications. RSC Adv, 2012, 2: 4364–4369
14 Zhang Y, Tang ZR, Fu X, *et al.* Engineering the unique 2D mat of graphene to achieve graphene-TiO_2 nanocomposite for photocatalytic selective transformation: What advantage does graphene have over its forebear carbon nanotube? ACS Nano, 2011, 5: 7426–7435
15 Zhang L, Hu X, Wang C, *et al.* Water-dispersible and recyclable magnetic TiO_2/graphene nanocomposites in wastewater treatment. Mater Lett, 2018, 231: 80–83
16 Shirai K, Fazio G, Sugimoto T, *et al.* Water-assisted hole trapping at the highly curved surface of nano-TiO_2 photocatalyst. J Am Chem Soc, 2018, 140: 1415–1422
17 Razali MH, Yusoff M. Highly efficient CuO loaded TiO_2 nanotube

photocatalyst for CO_2 photoconversion. Mater Lett, 2018, 221: 168–171
18 Pan X, Zhao Y, Liu S, *et al.* Comparing graphene-TiO_2 nanowire and graphene-TiO_2 nanoparticle composite photocatalysts. ACS Appl Mater Interfaces, 2012, 4: 3944–3950
19 Wang C, Zhang X, Zhang Y, *et al.* Hydrothermal growth of layered titanate nanosheet arrays on titanium foil and their topotactic transformation to heterostructured TiO_2 photocatalysts. J Phys Chem C, 2011, 115: 22276–22285
20 Li B, Xi B, Feng Z, *et al.* Hierarchical porous nanosheets constructed by graphene-coated, interconnected TiO_2 nanoparticles for ultrafast sodium storage. Adv Mater, 2018, 30: 1705788
21 Quan Q, Xie S, Weng B, *et al.* Revealing the double-edged sword role of graphene on boosted charge transfer versus active site control in TiO_2 nanotube arrays@RGO/MoS_2 heterostructure. Small, 2018, 14: 1704531
22 Sathish Kumar M, Yamini Yasoda K, Kumaresan D, *et al.* TiO_2-carbon quantum dots (CQD) nanohybrid: Enhanced photocatalytic activity. Mater Res Express, 2018, 5: 075502
23 Yang J, Wen Z, Shen X, *et al.* A comparative study on the photocatalytic behavior of graphene-TiO_2 nanostructures: Effect of TiO_2 dimensionality on interfacial charge transfer. Chem Eng J, 2018, 334: 907–921
24 Chen W, Li S, Chen C, *et al.* Self-assembly and embedding of nanoparticles by *in situ* reduced graphene for preparation of a 3D graphene/nanoparticle aerogel. Adv Mater, 2011, 23: 5679–5683
25 Long R, Casanova D, Fang WH, *et al.* Donor–acceptor interaction determines the mechanism of photoinduced electron injection from graphene quantum dots into TiO_2: π-Stacking supersedes covalent bonding. J Am Chem Soc, 2017, 139: 2619–2629
26 Zhang Y, Foster CW, Banks CE, *et al.* Graphene-rich wrapped petal-like rutile TiO_2 tuned by carbon dots for high-performance sodium storage. Adv Mater, 2016, 28: 9391–9399
27 Lee JS, You KH, Park CB. Highly photoactive, low bandgap TiO_2 nanoparticles wrapped by graphene. Adv Mater, 2012, 24: 1084–1088
28 Yu X, Liu W, Deng X, *et al.* Gold nanocluster embedded bovine serum albumin nanofibers-graphene hybrid membranes for the efficient detection and separation of mercury ion. Chem Eng J, 2018, 335: 176–184
29 Yu X, Zhang W, Zhang P, *et al.* Fabrication technologies and sensing applications of graphene-based composite films: Advances and challenges. Biosens Bioelectron, 2017, 89: 72–84
30 Kim H, Cho MY, Kim MH, *et al.* A novel high-energy hybrid supercapacitor with an anatase TiO_2-reduced graphene oxide anode and an activated carbon cathode. Adv Energy Mater, 2013, 3: 1500–1506
31 Deng W, Fang Q, Zhou X, *et al.* Hydrothermal self-assembly of graphene foams with controllable pore size. RSC Adv, 2016, 6: 20843–20849
32 Li K, Liu W, Ni Y, *et al.* Technical synthesis and biomedical applications of graphene quantum dots. J Mater Chem B, 2017, 5: 4811–4826
33 Marcano DC, Kosynkin DV, Berlin JM, *et al.* Improved synthesis of graphene oxide. ACS Nano, 2010, 4: 4806–4814
34 Sakthivel S, Neppolian B, Shankar MV, *et al.* Solar photocatalytic degradation of azo dye: Comparison of photocatalytic efficiency of ZnO and TiO_2. Sol Energy Mater Sol Cells, 2003, 77: 65–82
35 Atchudan R, Jebakumar Immanuel Edison TN, Perumal S, *et al.* Effective photocatalytic degradation of anthropogenic dyes using graphene oxide grafting titanium dioxide nanoparticles under UV-light irradiation. J PhotoChem PhotoBiol A-Chem, 2017, 333: 92–104

Acknowledgements This work was supported by the National Natural Science Foundation of China (NSFC, 51573013 and 51873016) and the Open Project Program of Beijing Key Laboratory of Quality Evaluation Technology for Hygiene and Safety of Plastics, Beijing Technology and Business University (QETHSP2019006).

Author contributions Zhang X, Wen B, and Su Z designed the project; Wei W, Zhang X, and Zhang S performed the experiments; Zhang X and Wei W wrote the paper with support from Wen B and Su Z. All authors contributed to the general discussion.

Conflict of interest The authors declare no conflict of interest.

Zhiqiang Su was born in 1975 and obtained his PhD degree in 2005 at the Institute of Chemistry, Chinese Academy of Sciences. After a post-doctoral stay at Tsinghua University, he joined Beijing University of Chemical Technology in 2007 and was appointed as full professor in 2012. In 2011 he worked at Friedrich-Schiller-University Jena, Germany as an experienced research fellow of Alexander von Humboldt Foundation. His research interest includes nanohybrids, biomedical materials, biosensors, and bioelectronics. So far, he has published more than 100 peer-reviewed papers with 3300 citations. His H-index is 35.

氧化石墨烯基3D泡沫的制备策略、界面协同机理和高效光催化性能研究

张晓媛[1†], 魏文锋[1†], 张山[1], 温变英[2*], 苏志强[1*]

摘要 本文通过高效低成本的水热法将TiO_2@CQDs插入还原氧化石墨烯片层间, 制备了一种独特的纳米杂化三维rGO-TiO_2-CQDs泡沫. 在氙灯照射下, 所合成的三维rGO-TiO_2-CQDs泡沫对甲基橙(MO)、亚甲蓝(MB)以及罗丹明B(RhB)表现出很高的降解速率, 在多次使用后仍然保持高效且形貌不变. 这种优异的光催化性能归因于rGO-TiO_2-CQDs泡沫的多孔结构, 以及密集吸附在石墨烯表面上的催化剂TiO_2@CQDs. 本文中所描述的三维杂化泡沫将光催化剂TiO_2与半导体石墨烯和碳量子点结合, 有望为进一步提高电荷分离效率, 进而提高光催化效果, 开辟一条新途径.

